ISSN 1674-1056
http://cpb.iphy.ac.cn
http://iopscience.iop.org/cpb
中国物理 B
Chinese Physics
中国物理 Chinese Physics B

Band offset and electronic properties at semipolar plane AlN(1101)/diamond heterointerface

Kong-Ping Wu(吴孔平), Wen-Fei Ma(马文飞), Chang-Xu Sun(孙昌旭), Chang-Zhao Chen(陈昌兆), Liu-Yi Ling(凌六一), Zhong-Gen Wang(王仲根)
Citation: Chin. Phys. B . 2018, 27(5): 058101. **doi:** 10.1088/1674-1056/27/5/058101

Journal homepage: http://cpb.iphy.ac.cn; http://iopscience.iop.org/cpb

What follows is a list of articles you may be interested in

Synthesis of strong SiV photoluminescent diamond particles on silica optical fiber by chemical vapor deposition

Zongchun Yang(仰宗春), Yingshuang Mei(梅盈爽), Chengke Chen(陈成克), Yinlan Ruan(阮银兰), Xiaojun Hu(胡晓君)
Chin. Phys. B . 2018, 27(3): 038101. **doi:** 10.1088/1674-1056/27/3/038101

Thermal conduction of one-dimensional carbon nanomaterials and nanoarchitectures

Haifei Zhan(占海飞), Yuantong Gu(顾元通)
Chin. Phys. B . 2018, 27(3): 038103. **doi:** 10.1088/1674-1056/27/3/038103

Synthesis of diamonds in Fe—C systems using nitrogen and hydrogen co-doped impurities under HPHT

Shi-Shuai Sun(孙士帅), Zhi-Hui Xu(徐智慧), Wen Cui(崔雯), Xiao-Peng Jia(贾晓鹏), Hong-An Ma(马红安)
Chin. Phys. B . 2017, 26(9): 098101. **doi:** 10.1088/1674-1056/26/9/098101

Different effect of NiMnCo or FeNiCo on the growth of type-IIa large diamonds with Ti/Cu as nitrogen getter

Shang-Sheng Li(李尚升), He Zhang(张贺), Tai-Chao Su(宿太超), Qiang Hu(胡强), Mei-Hua Hu(胡美华), Chun-Sheng Gong(龚春生), Hon-An Ma(马红安), Xiao-Peng Jia(贾晓鹏), Yong Li(李勇)
Chin. Phys. B . 2017, 26(6): 068102. **doi:** 10.1088/1674-1056/26/6/068102

Synthesis of N-type semiconductor diamonds with sulfur, boron co-doping in FeNiMnCo-C system at high pressure and high temperature

He Zhang(张贺), Shangsheng Li(李尚升), Taichao Su(宿太超), Meihua Hu(胡美华), Hongan Ma(马红安), Xiaopeng Jia(贾晓鹏), Yong Li(李勇)
Chin. Phys. B . 2017, 26(5): 058102. **doi:** 10.1088/1674-1056/26/5/058102

Band offset and electronic properties at semipolar plane AlN(1 $\bar{1}$01)/diamond heterointerface*

Kong-Ping Wu(吴孔平)†, Wen-Fei Ma(马文飞), Chang-Xu Sun(孙昌旭), Chang-Zhao Chen(陈昌兆), Liu-Yi Ling(凌六一), and Zhong-Gen Wang(王仲根)

School of Electrical and Information Engineering, Anhui University of Science and Technology, Huainan 232001, *China*

(Received 4 January 2018; revised manuscript received 11 March 2018; published online 26 April 2018)

Tailoring the electronic states of the AlN/diamond interface is critical to the development of the next-generation semiconductor devices such as the deep-ultraviolet light-emitting diode, photodetector, and high-power high-frequency field-effect transistor. In this work, we investigate the electronic properties of the semipolar plane AlN(1 $\bar{1}$01)/diamond heterointerfaces by using the first-principles method with regard to different terminated planes of AlN and surface structures of diamond (100) plane. A large number of gap states exist at semi-polar plane AlN(1 $\bar{1}$01)/diamond heterointerface, which results from the N 2p and C 2s2p orbital states. Besides, the charge transfer at the interface strongly depends on the surface termination of diamond, on which hydrogen suppresses the charge exchange at the interface. The band alignments of semi-polar plane AlN(1 $\bar{1}$01)/diamond show a typical electronic character of the type-II staggered band configuration. The hydrogen-termination of diamond markedly increases the band offset with a maximum valence band offset of 2.0 eV and a conduction band offset of 1.3 eV for the semi-polar plane N–AlN(1 $\bar{1}$01)/hydrogenated diamond surface. The unique band alignment of this Type-II staggered system with the higher CBO and VBO of the semi-polar AlN/HC(100) heterostructure provides an avenue to the development of robust high-power high-frequency power devices.

Keywords: diamond, heterointerface, charge transfer, band offset

PACS: 81.05.ug, 73.20.At, 81.05.Ea, 74.25.F– **DOI:** 10.1088/1674-1056/27/5/058101

1. Introduction

Diamond (C) has attracted wide interest as an extreme semiconductor material for next-generation power and photoelectronic devices due to the wide bandgap, the highest thermal conductivity, highest breakdown field, highest carrier mobility, and highest carrier saturation velocity in all the available semiconductors.[1] The practical application of semiconductor diamond electronic devices relies on the reduction of the electrical resistivity of diamond by doping impurities and controlling the interface formed between diamond and other material. Despite the lack of shallow dopant at this moment, the hydrogenated diamond surface exhibits a unique p-type surface conductivity with a hole density of around 10^{13} cm^{-2}.[2] Such a surface conductivity has opened the avenue to the development of metal-semiconductor or metal-oxide-semiconductor field-effect transistors (FETs), which showed exciting performance with either high cut-off frequency or capability operating at elevated temperatures.[3,4] Another important structure is the hetero pn-junction, which is the basis of the development of deep-ultraviolet photoelectronic and power devices.[5] Among all these heterostructures, the interface properties at the junctions of diamond with other materials determine the ultimate device performances.

One promising junction is the AlN/C heterostructure, in which both AlN and diamond are wide-bandgap semiconductors. The AlN/C heterostructure is expected to lead to a variety of novel semiconductor devices such as deep-ultraviolet (DUV) light emitting diode, DUV photodetector, and high-power FET. Experimentally, the implementations of AlN/C pn-junction diode and field-effect transistors have already been demonstrated.[6–8] Although single-crystal AlN epitaxial layer on diamond could be achieved, the existence of a large number of interface states is anticipated due to the large lattice mismatch between the hexagonal AlN and the cubic diamond. The high concentration defects degrade the device performances such as the occurrences of sub-bandgap emission and the low efficiency of band-to-band recombination in pn-junction diode and high leakage current in the electronic device. Therefore, the understanding of the interface characteristics of the AlN/C heterojunction is in demand for the development of the next-generation optoelectronic devices operating at DUV region and electronic devices for high-power and high-frequency applications.

However, few experimental values[7] or theoretical results[9,10] are available in the interface characteristic parameters of the AlN/C heterostructure. The reported calculations are only limited to the band offset of polar plane AlN(0001)/C, and the investigations on the electronic properties at the interface of semi-polar plane AlN(1 $\bar{1}$01)/C heterostructure is still

*Project supported by the Scholarship Council of China (Grant No. 201508340047), the Postdoctoral Science Foundation of China (Grant No. 2016M601993), the Postdoctoral Science Foundation of Anhui Province, China (Grant No. 2017B215), and the Anhui Province University Outstanding Talent Cultivation Program, China (Grant No. gxfxZD2016077).

†Corresponding author. E-mail: kongpingwu@126.com

© 2018 Chinese Physical Society and IOP Publishing Ltd

lacking. In order to fully realize the electronic properties such as the electronic structure, band-offset, and charge transfer at the AlN/C interface, the details at the interface, such as the atomic structure, composition, crystal orientation, and polarity, should be theoretically investigated.

For chemical vapor deposition (CVD) single-crystal diamond, the most important crystallographic surface is the (100) surface, on which most of the homoepitaxial growths and devices fabrication have been performed. Due to the existence of dangling bonds, the (100) surface appears with a 2×1-(100) surface reconstruction for the clean surface (C(100)) and 2×1-(100):H reconstruction for the surface with hydrogen termination (HC(100)).[11–14] Another feature of H-diamond is the negative electron affinity,[15] which allows the formation of a high interface barrier for diamond heterojunction devices and facile electron emitting source.

In this paper, we systematically investigate the interfacial characteristics of the semi-polar plane AlN(1 $\bar{1}$01)/C heterostructures by considering the effects of the terminated planar (N terminated planar (N–AlN), Al terminated planar (Al-AlN)), the surface structure of diamond, and the atomic bonds at the interfaces by using the first-principles study. The different diamond surfaces such as the clean reconstructed 2×1-(100) surface (C(100)) and H-terminated diamond 2×1-(100) surface (HC(100)) are examined. The effects of the atomic structures of C–N bonding and C–Al bonding at the interface are also analyzed. The density of states, band alignments, charge transfer, and bonding mechanism of the AlN/C are calculated and analyzed. In addition, the N-vacancy (V_N) is the most stable native defect in AlN bulk,[16,17] which will bring a change of the carrier concentration when the N is absent in AlN single crystal. Its effect on the band offset at the N–AlN/C(100) heterointerface is also considered in this work.

2. Computational and modeling details

2.1. Atomic structure of the interface

For diamond, the theoretical equilibrium constant of 3.53 Å was used in the interfacial calculation for consistency. The clean and hydrogen-terminated reconstructed 2×1-(100) surface slabs are illustrated in Figs. 1(a) and 1(b), respectively, which are optimized for the calculations. The total density of states (TDOS) of the C(100) reveals the metallic characters, which is mainly related to dangling bond orbital on the dimer atoms, while the TDOS of hydrogenated diamond HC(100) surface still preserves the semiconducting nature. These are in good agreement with the previous computational results.[18,19] For AlN, the theoretical equilibrium value of the lattice constant of 3.08 Å is used. In order to minimize the interface mismatch, the AlN/C hetero-structure slab is obtained by matching an AlN (1 $\bar{1}$01) slab to the reconstructed 2×1-(100) surface. The relative basis vectors ($\boldsymbol{u}'$, $\boldsymbol{v}'$) of AlN(1 $\bar{1}$01) surface are extracted through the coordinate transformation of the origin basis vectors ($\boldsymbol{u}$ and $\boldsymbol{v}$). The process of coordinate transformation is shown in Fig. 1(c). Finally, the slab of AlN(1 $\bar{1}$01) surface is shown in Fig. 1(d). Besides, lattice constants x and y at the in-plane correspond to the average of lattice constants for both the AlN(1 $\bar{1}$01) slab and the reconstructed diamond 2×1-(100) surface, resulting in a 3.0% tensile strain on the diamond side and a 3.0% compressive strain on AlN side.

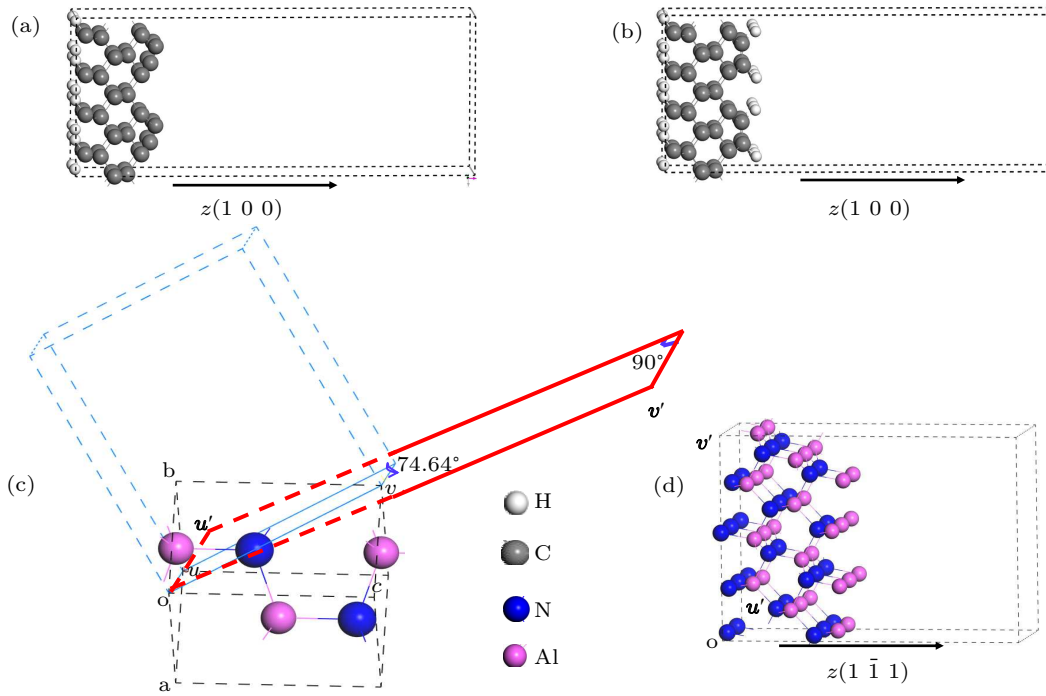


Fig. 1. (color online) Side view of (a) clean diamond (100)-2×1 and (b) hydrogenated diamond (100)-2×1:H surface. Processes of extracting relative basis vectors ($\boldsymbol{u}'$, $\boldsymbol{v}'$) from (c) origin basis vectors and (d) slab of AlN(1 $\bar{1}$01) surface.

Four kinds of atomic bonding configurations at the interface are calculated, and configurations are N–AlN(1 $\bar{1}$01)/HC(100) (Fig. 2(a)), Al–AlN(1 $\bar{1}$01)/HC(100) (Fig. 2(b)), N–AlN(1 $\bar{1}$01)/C(100) (Fig. 2(c)), and Al–AlN(1 $\bar{1}$01)/(100) (Fig. 2(d)), corresponding to interfaces containing the C–H–N, C–H–Al, C–N, and C–Al constituents, respectively. Here, the surface of diamond is the reconstructed 2 × 1-(100) surface with or without hydrogen, and the AlN(1 $\bar{1}$01)/C hetero-structure slab contains 6 layers of C atoms and 4 layers of Al–N.

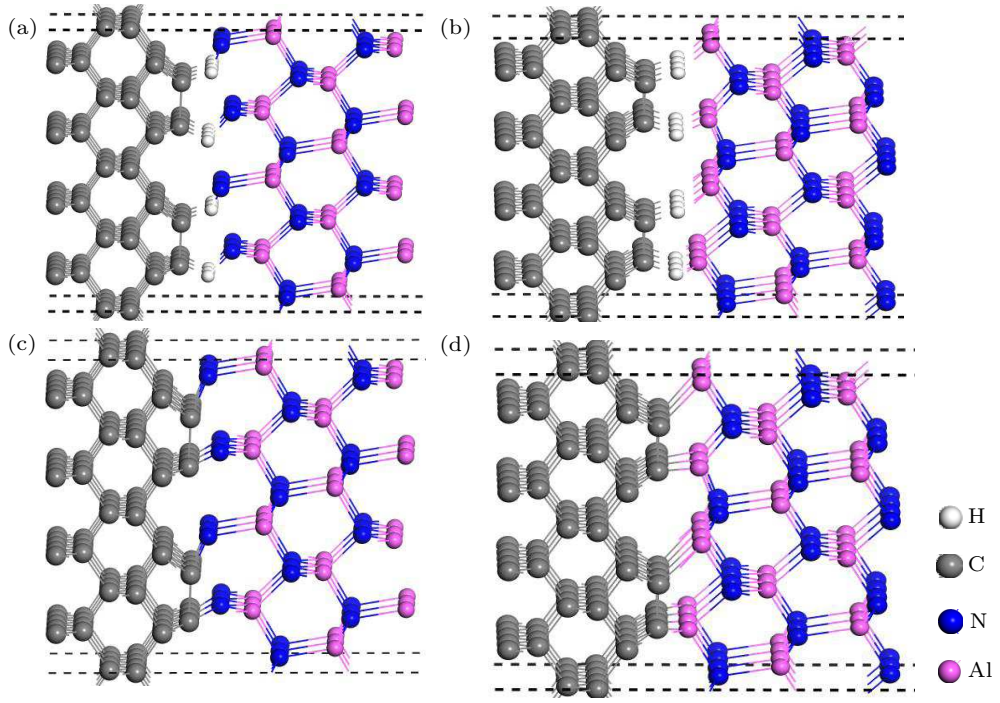


Fig. 2. (color online) Slab models of polar AlN(1 $\bar{1}$01)/HC interfaces with (a) N–AlN(1 $\bar{1}$01)/HC(100) and (b) Al–AlN(1 $\bar{1}$01)/HC(100) respectively, and slab models of AlN(1 $\bar{1}$01)/C interface with (c) N–AlN(1 $\bar{1}$01)/C(100) and (d) Al–AlN(1 $\bar{1}$01)/C(100) respectively.

2.2. Methods

The total-energy and physical properties were calculated with Vienna *abinitio* Simulation Package (VASP 5.3.3) based on density-functional theory (DFT) within the generalized gradient approximation (GGA).[20,21] The projector-augmented wave pseudo-potentials and the exchange–correlation functional of Perdew, Burke, and Ernzerhof (PBE) for the GGA were utilized in the simulation.[22] Valence electron configurations for the elements were $2s^2 2p^2$ for C, $3s^2 3p^1$ for Al, and $2s^2 2p^3$ for N. The Monkhorst–Pack scheme was employed for the Brillouin zone integration with a 5 ×9 × 1 *k*-point mesh.[23] At the same time, the three bottom layers of C atoms and a layer of H atoms were fixed, whereas the others moved freely, in order to facilitate the simulation of a thick diamond substrate and eliminate any strain or stress in the lattice structure as much as possible. After geometry optimization, the interface distance (the distances of C–N, H–N, C–Al, and H–Al along the *z*-direction) between diamond and AlN was determined by minimizing the total energies of the configurations.[24,25]

The plane wave basis set is included and truncated with a cut-off energy of 500 eV, and the electronic total energy is well converged to 10^{-6} eV/cell with respect to the *k*-point sampling. The relaxation of the atomic structure is carried out using the calculated Hellmann–Feynman forces until the force on each relaxed atom is less than 0.01 eV/Å. Finally, a dipole correction is included in the middle of the vacuum to compensate for the spurious electrostatic interactions of the asymmetric slab with a non-vanishing surface-dipole moment.[26–28] Pseudo-hydrogen atoms $^{3/4}$H and $^{5/4}$H[29] are chosen to passivate the dangling bonds of N and Al atoms at the (1 $\bar{1}$01) surface, respectively. Besides, a 20-Å-thick vacuum layer is added to separate the surfaces in adjacent cells in the z-direction to eliminate the interactions between them. As a general rule for calculating the physical properties of the heterostructure, van der Waals correction (vdW-DF)[30] is used to test the effect of the nonbonding forces on interface adhesion formation energy.

3. Results and discussion

3.1. Interface adhesion formation energy

To discuss the thermodynamic stability of the four types of heterostructures, the interface adhesion formation energy is calculated according to the following relationship:[31]

$$E_{\text{adh}} = E_{\text{AlN/C}} - E_{\text{AlN}} - E_{\text{C}}, \tag{1}$$

where $E_{\mathrm{AlN/C}}$, E_{AlN}, and E_{C} represent the total energies of AlN(1 $\bar{1}$01)/C heterostructure, the corresponding part of the AlN(1 $\bar{1}$01) and C(100) slab, respectively. The total energies of AlN(1 $\bar{1}$01) and C(100) slab are calculated with the same unit cell size, number of K-points, and cutoff energy as those of AlN(1 $\bar{1}$01)/C heterostructures. The calculated interface adhesion formation energies are −1.36, 4.82, −9.21, and −6.34 eV corresponding to the the N–AlN(1 $\bar{1}$01)/HC(100), Al–AlN(1 $\bar{1}$01)/HC(100), N–AlN(1 $\bar{1}$01)/C(100), and Al–AlN(1 $\bar{1}$01)/C(100) heterostructures, respectively. After considering the influence of der Waals (vdW) interaction, the corresponding interface adhesion formation energies change into −1.73, 5.12, −9.32, and −6.59 eV. In these heterostructures, the vdW interaction does not alter the interface adhesion formation energy too much. This slight difference between the PBE and vdW-DF results indicates that the vdW interaction plays a minor role in the four examined hetero-interfaces. Therefore, in the following, all electronic properties are calculated without the vdW correction. The positive formation energy indicates that the interface of Al–AlN(1 $\bar{1}$01)/HC(100) is not stable, while N–AlN(1 $\bar{1}$01)/C(100) is the most stable interface among the four types of heterostructure energetically. Later, we will not show the calculated data for the case of Al–AlN(1 $\bar{1}$01)/HC(100) interface. In the present calculations, the order of stability for the four types of AlN/C hetero-structures is as follows: N–AlN(1 $\bar{1}$01)/C(100)>Al–AlN(1 $\bar{1}$01)/C(100)>N–AlN(1 $\bar{1}$01)/HC(100)>Al–AlN(1 $\bar{1}$01)/HC(100). The calculation also discloses that the introduction of H at the interface weakens the stability for the AlN(1 $\bar{1}$01)/C heterostructure.

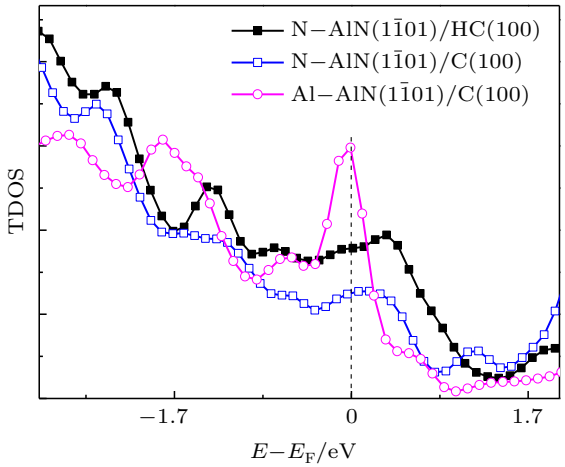


Fig. 3. (color online) Calculated total densities of states of N–AlN(1 $\bar{1}$01)/HC(100), N–AlN(1 $\bar{1}$01)/C(100), and Al–AlN(1 $\bar{1}$01)/C(100) heterostructures, with a vertical dashed line indicating Fermi level.

3.2. Electronic properties of interfaces

The calculated total densities of states (TDOSs) of the interfaces of N–AlN(1 $\bar{1}$01)/HC(100), N–AlN(1 $\bar{1}$01)/C(100), and Al–AlN(1 $\bar{1}$01)/C(100) heterostructures are shown in Fig. 3. In all these cases, metallic features at the interfaces are observed. Especially, for the Al–AlN(1 $\bar{1}$01)/C(100) interface, a dramatic increase of the TDOS near Fermi level is observed. To further understand the spatial evolution of the electronic structure of the AlN(1 $\bar{1}$01)/C heterostructure from the interface to the surface, we calculate the projected density of states (PDOS) layer by layer as shown in Figs. 4(a)–4(c) corresponding to the N–AlN(1 $\bar{1}$01)/HC(100), N–AlN(1 $\bar{1}$01)/C(100), and Al–AlN(1 $\bar{1}$01)/C(100) interfaces, respectively. The PDOS is calculated by averaging the total DOS per layer (LTDOS) for each atom in the layer. To clearly identify the electronic states,

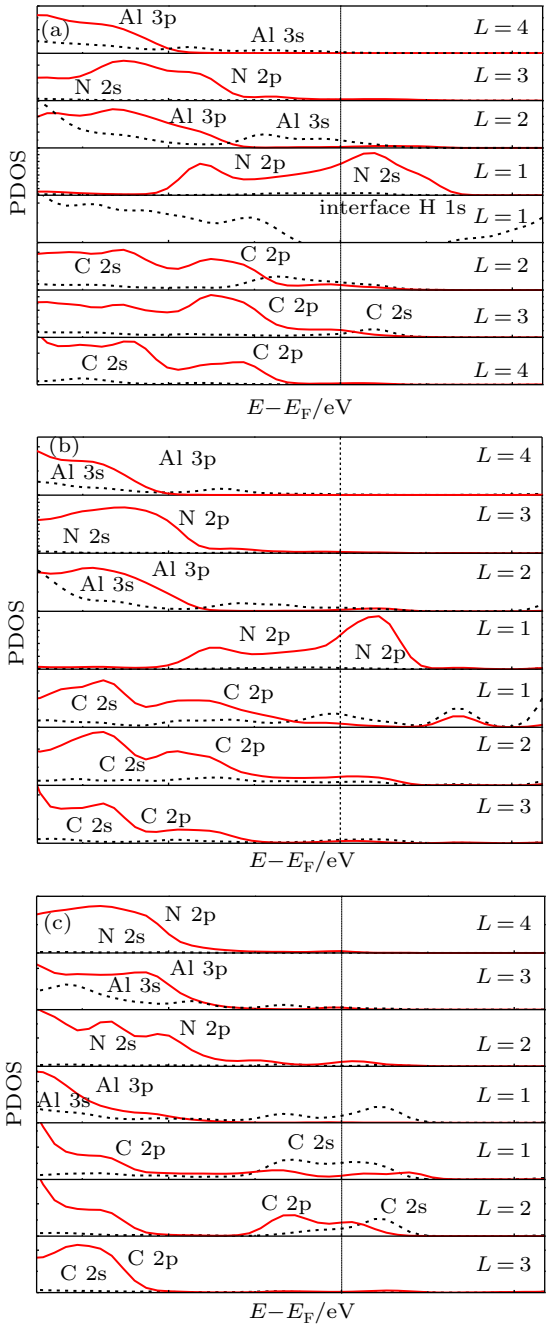


Fig. 4. (color online) Calculated atomic projected densities of states layer by layer for (a) N–AlN(1 $\bar{1}$01)/HC(100), (b) N–AlN(1 $\bar{1}$01)/C(100), and (c) Al–AlN(1 $\bar{1}$01)/C(100). L denotes the number of atomic layers and increases with increasing separation from the interface. The vertical dashed line refers to Fermi level.

the PDOSs of the heterostructures are calculated by starting from the interface region and extending to the bulk AlN and the diamond regions. The L denotes the number of the atomic layers and increases with increasing separation from the interface.

Figure 4(a) illustrates the PDOS of the N–AlN(1 $\bar{1}$01)/HC(100) heterostructure, in which the interface states mainly result from the interaction between the atoms near the interface. The interface states are contributed from the C 2s2p, and N 2p, Al 3s orbitals as shown Fig. 4(a). It is revealed that the interaction among the atoms at the interface occurs mainly within two C atom layers in diamond for the N–AlN(1 $\bar{1}$01)/HC(100) heterostructure, and the electronic properties turn into the feature of the bulk diamond after the third C atom layer. Such a trend in the PDOS varying with increasing atomic layer (L) is similar to those for the other two interfaces of the N–AlN(1 $\bar{1}$01)/C(100) and Al–AlN(1 $\bar{1}$01)/C(100) interfaces, in which the PDOSs are composed of C 2s2p and N 2p, and C 2s2p, N 2p and Al 3s orbital contribution, respectively. Therefore, for the interfaces of N–AlN(1 $\bar{1}$01)/C(100) and Al–AlN(1 $\bar{1}$01)/C(100) heterostructures as shown Figs. 4(b) and 4(c), a large number of electronic states appear in the band gap due to the strong interaction between C 2s2p and N 2p or Al 3s near the interface, forming the interface states.

3.3. Charge transfer

In order to further disclose the bonding mechanism and the transfer of electrons between the adjacent layers at the interface of the AlN(1 $\bar{1}$01)/C heterostructure, plane-averaged electron density difference $\Delta\rho(z)$ along the direction perpendicular to the interface is calculated. The electron density difference $\Delta\rho(x,y,z)$ is described as[32,33]

$$\Delta\rho(x,y,z) = \rho(\mathrm{AlN}(1\,\bar{1}01)/\mathrm{C}(100)) - (\rho(\mathrm{C}(100)) + \rho(\mathrm{AlN}(1\,\bar{1}01))), \quad (2)$$

where ρ(AlN(1 $\bar{1}$01)/C(100)) is the electron density of the AlN(1 $\bar{1}$01)/C(100) heterostructure, and ρ(C(100)) and ρ(AlN(1 $\bar{1}$01)) are the electron densities of the reconstructed diamond 2 × 1-C(100) surface and AlN (1 $\bar{1}$01) surface with exactly the same geometries as the AlN(1 $\bar{1}$01)/C(100) heterostructure, respectively.

Figures 5(a)–5(c) show the contours of the calculated charge density differences for the interfaces of N–AlN(1 $\bar{1}$01)/HC(100), N–AlN(1 $\bar{1}$01)/C(100), and Al–AlN(1 $\bar{1}$01)/C(100), respectively. Figure 5(a) shows the characteristics of charge transfer for N–AlN(1 $\bar{1}$01)/HC(100) heterostructure. It is clearly seen that charge is depleted in the region of Al plane, meanwhile, the charge is accumulated in the region of N plane near the interface. The charge is depleted near the H atoms, which is not shown in the cleaved plane in this calculation. In particular, for the C plane, the charge is depleted near some C atoms and charge is also accumulated near the other C atoms in the first and second layers. Therefore, C–H, C–C, and C–N bonds probably exist at this interface. A similar phenomenon of charge transfer is also observed in N–AlN(1 $\bar{1}$01)/C(100) and Al–AlN(1 $\bar{1}$01)/C(100) hetero-structures as shown in Figs. 5(b) and 5(c). Comparing the charge transfer in Fig. 5(a) with that in Fig. 5(c), the hydrogen termination on diamond surface weakens the charge transfer from C to N, which is also an important reason for the instability of Al–AlN(1 $\bar{1}$01)/HC(100) heterostructure. It is disclosed that the hybridization takes place between C 2s2p and N 2p from the PDOS as shown in Fig. 4(a), and a chemical bonding near the interface is formed, thus stabilizing the interface. The charge transfer only takes place among C, H, N, and Al atoms within three atomic layers near the interface, which indicates a strong localization character.

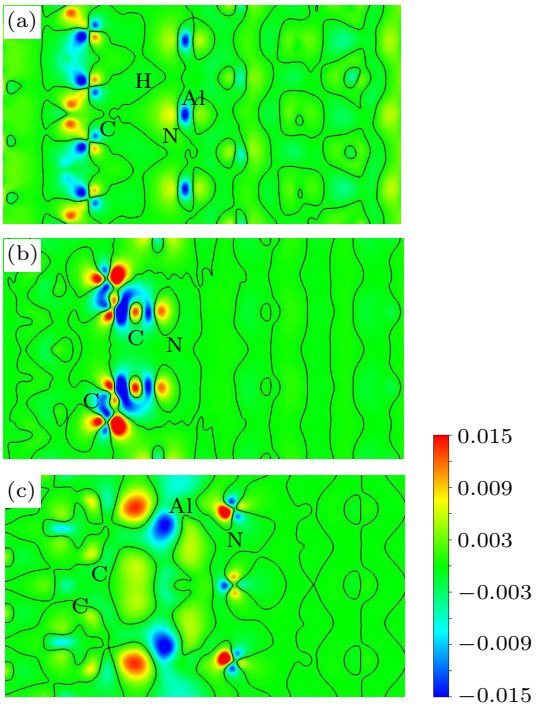


Fig. 5. (color online) Contour plots of valence electronic-charge density difference for interfaces of (a) N–AlN(1 $\bar{1}$01)/HC(100), (b) N–AlN(1 $\bar{1}$01)/C(100), and (c) Al–AlN(1 $\bar{1}$01)/C(100) taken along the (100) plane. Atoms that intersect the contour plane are labeled (blue: charge is depleted, red: charge is accumulated).

To further analyze the charge transfer quantitatively, the plane-averaged (x, y) charge density difference $\Delta\rho(z)$ for interfaces of N–AlN(1 $\bar{1}$01)/HC(100), N–AlN(1 $\bar{1}$01)/C(100), and Al–AlN(1 $\bar{1}$01)/C(100) heterostructures are calculated and shown in Figs. 6(a)–6(c), respectively. The magnitude of charge transfer (q) is calculated by integrating $\Delta\rho(z)$ over the full z range. The plane-averaged (x, y) charge density difference for the AlN(1 $\bar{1}$01)/C hetero-structure deviates from zero near the interface, suggesting that a considerable number of charge transfer between the diamond and AlN(1 $\bar{1}$01)

slabs. As shown in Figs. 6(a) and 6(c) for the interfaces of N–AlN(1 $\bar{1}$01)/HC(100) and N–AlN(1 $\bar{1}$01)/C(100) heterostructures, charge is observed to be depleted noticeably in the C or H and Al atoms the first nearest to the interface, and accumulated in N atoms the first nearest to the interface. In the case of Al–AlN(1 $\bar{1}$01)/C(100) hetero-structure as shown in Figs. 6(c), the charge is observed to be depleted noticeably in the C atoms that are the second nearest to the interface Al atoms and accumulated in the C atoms that are the first nearest to the interface. The charge depletion and accumulation are determined by the electronegativity, which is higher for N atoms than for C atoms. It is revealed that the atoms that are the second nearest to the interface contribute to the interfacial bonding. It is observed that the introduction of H plays a role in suppressing the charge transfer between AlN(1 $\bar{1}$01) and diamond. The value of charge transfer decreases from 0.037e to 0.025e as shown in Figs. 6(a) and 6(b).

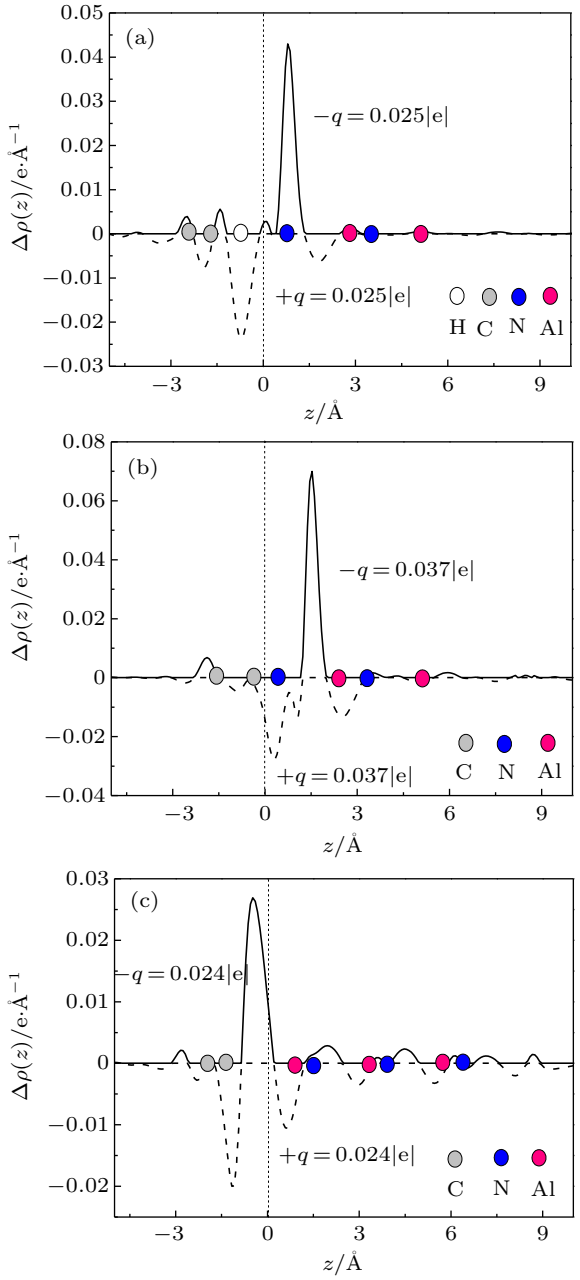


Fig. 6. (color online) Curves of plane-averaged electron density difference, $\Delta\rho(z)$, for systems (a) N–AlN(1 $\bar{1}$01)/HC(100) and (b) N–AlN(1 $\bar{1}$01)/C(100) and (c) Al–AlN(1 $\bar{1}$01)/C(100). Atom positions are indicated by solid circles, and q refers to charge transfer calculated by integrating $\Delta\rho(z)$ over the full z range. The vertical dashed line indicates interface.

3.4. Band alignment

The energy band discontinuities or band offsets at the interfaces are also calculated. Usually, there are two methods to evaluate the band offset at the interface. One is the well-established "bulk plus lineup" method[34–36] in which the macroscopic averaged electrostatic potentials are used as reference energies as proposed by van de Walle *et al.*[37] The other is determined directly from the site projected density of states (PDOS), in which the valence band offset at the interface is the energy difference between the tops of the valence bands of the AlN layer and the diamond layer.[38–40] Although this method can determine the band offset directly, the results are usually sensitive to the computational condition such as the number of K-points, cut-off energy, size of a supercell, etc. Once the alignment of the valence-band edge (E_V) and Fermi level (E_F) can be obtained, the conduction-band edge (E_C) is calculated by the reliable experimental band-gap values.

Here, the band offsets are calculated by the reference macroscopically-averaged electrostatic potential method. In general, the energy of the valence band offset (E_{VBO}) can be expressed as the sum of two terms[34–36]

$$E_{VBO} = \Delta E_V + \Delta V, \tag{3}$$

where the term of ΔV is related to the lineup of the macroscopically-averaged electrostatic potential, and ΔE_V is the energy difference between the relevant valence band edges ($\Delta E_{diamond}$ and ΔV_{AlN}), when the single-particle eigenvalues are measured with respect to macroscopically-averaged electrostatic potential in the buck diamond and the buck AlN, respectively. Due to lattice mismatch between diamond and AlN, ΔE_V is calculated for buck diamond and AlN under a strain of 3% corresponding to the lattice parameters of the hetero-structure slab.

The planar average values of the electrostatic potentials for interfaces of N–AlN(1 $\bar{1}$01)/HC(100), N–AlN(1 $\bar{1}$01)/C(100), and Al–AlN(1 $\bar{1}$01)/C(100) heterostructures are calculated and shown in Figs. 7(a)–7(c), respectively. Each potential is an oscillating function of z that corresponds to the atomic plane. A macroscopic average value of electrostatic potentials as a function of z is calculated as shown in Fig. 7. The calculated results of lineup term (ΔV) and valence band offset (VBO) are displayed in Fig. 7. As shown in

Fig. 7(a), the VBO equals 2.0 eV for N–AlN(1 $\bar{1}$01)/HC(100) heterostructure, more than doubled VBO value (0.7 eV) of the N–AlN(1 $\bar{1}$01)/C(100) heterostructure. However, for the Al–AlN(1 $\bar{1}$01)/C(100) heterostructure, the VBO value is 1.5 eV as shown in Fig. 7(c). The terminal surface of AlN has also a nontrivial effect on the valence band offset. The VBO value (0.7) of the N–AlN(1 $\bar{1}$01)/C(100) heterostructure with C–N polar interface is less than the VBO value (1.5 eV) of the Al–AlN(1 $\bar{1}$01)/C(100) heterostructure with C–Al polar interface. Besides, the hydrogen-termination of diamond also greatly increases the VBO to 2.0 eV from a clean diamond surface VBO value 0.7 eV.

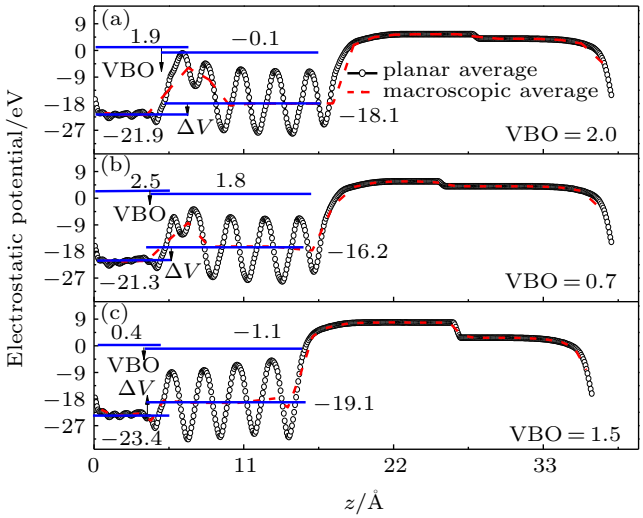


Fig. 7. (color online) Planar electrostatic potentials exhibiting lattice plane oscillations for (a) N–AlN(1 $\bar{1}$01)/HC(100), (b) N–AlN(1 $\bar{1}$01)/C(100), and (c) Al–AlN(1 $\bar{1}$01)/C(100), which are filtered out by macroscopic averaging (red dashed line). The valence band tops of diamond and AlN are evaluated with respect to the macroscopic average electrostatic potentials of the strained diamond and AlN, respectively.

According to the obtained VBOs at the interfaces, the relative position of valence band and conduction-band edges of N–AlN(1 $\bar{1}$01)/HC(100), N–AlN(1 $\bar{1}$01)/C(100), and Al–AlN(1 $\bar{1}$01)/C(100) as obtained from the "bulk plus lineup" method are schematically displayed in Figs. 8(a)–8(c), respectively. Here, the experimental band-gap values of diamond (5.5 eV)[41,42] and AlN (6.2 eV)[43,44] are used to calculate the CBO. The results reveal that the largest band offsets (VBO (2.0 eV), CBO (1.3 eV)) exist at the interface of the N–AlN(1 $\bar{1}$01)/HC(100), while the lowest band offsets (VBO (0.7 eV), CBO (0 eV)) are obtained at the interface of the N–AlN(1 $\bar{1}$01)/C(100). Each of all the AlN/C hetero-structures shows that it has a typical electronic character of the type-II staggered band configuration. Beside, by gradually reducing the interfacial N content from 100% to 75% at the interface of the N–AlN(1 $\bar{1}$01)/C(100), the valence band offsets increase from 0.7 eV for the interface of the N–AlN(1 $\bar{1}$01)/C(100) and from 0.9 eV for the interface with V_N to 1.0 eV for the interface with $2V_N$, respectively.

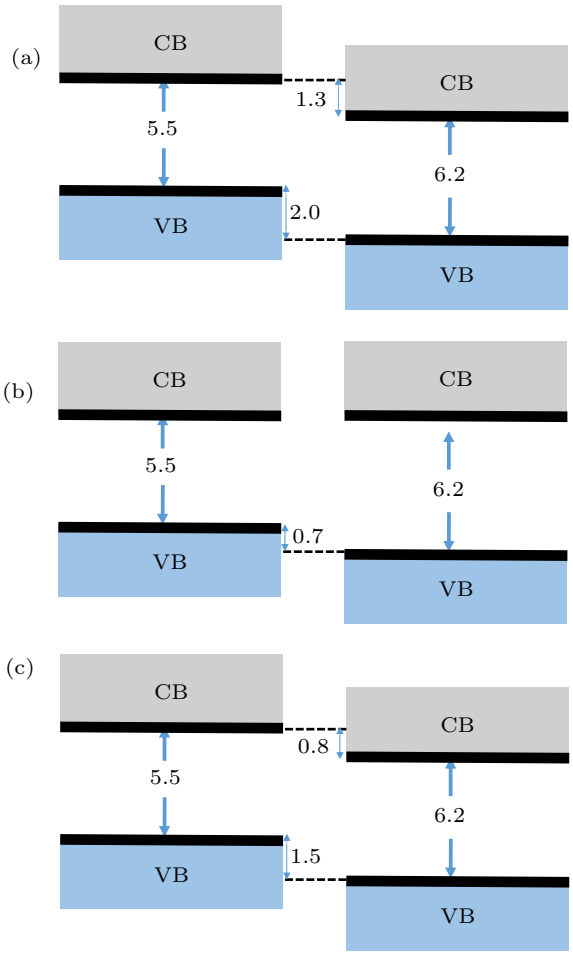


Fig. 8. (color online) Schematic representations of relative position of valence band and conduction-band edges of (a) N–AlN(1 $\bar{1}$01)/HC(100), (b) N–AlN(1 $\bar{1}$01)/C(100), and (c) Al–AlN(1 $\bar{1}$01)/C(100) as obtained from the "bulk plus lineup" method.

The computed band offsets for AlN(1 $\bar{1}$01)/C heterostructures are summarized in Table 1 showing their comparison with the experimental results. According to experimental values of the electron affinity of AlN and diamond,[45,46] the VBO values can also be estimated to range from 0.45 eV to 3.3 eV. In our calculation, the minimum and maximum VBO values are 0.7 and 2.0 eV, respectively, depending on the details of the interface structure. The introduction of hydrogen into the diamond surface dramatically increases the VBO and CBO values. This is in good agreement with the fact that the electron affinity of AlN with Al-termination is higher than that of AlN with N-termination,[47] and also consistent with the negative affinity of the hydrogenated diamond surface. Our data are in discrepancy with the theoretical calculations by Silvestri *et al.*,[10] where VBO values were 1.6 eV for the interface with C–N constituents and 0.6 eV for the interface with C–Al constituents, respectively. This inconsistency possibly relates to the AlN semipolar surface as well as the selection of the diamond surface structure, which is diamond $2 \times 1(100)$ reconstruction surface in our case and diamond $1 \times 1(100)$ surface in Ref. [10].

Table 1. Valence band offset (VBO) and conduction band offset (CBO) values calculated by "bulk plus lineup" method. For VBO and CBO, a positive number indicates that valence band top and conduction band minimum of the diamond are higher than those of the AlN.

Heterostructure	Interface atoms	Formation energy	VBO	CBO	Memo
Semi-polar AlN(1 $\bar{1}$01)/C(100)	C–H–N	−1.36	2.0	1.3	
	C–H–Al	4.82	–	–	not stable
	C–N	−9.21	0.7	0.0	
	C–Al	−6.34	1.5	0.8	
Ref. [10]	–	–	0.63 to 1.60	−0.07 to 0.90	theory
Ref. [2]	–	–	4.0	3.5	experimental
Ref. [46]	–	–	2.1	1.37	experimental
Ref. [48]	–	–	0.45	−0.28	experimental

4. Conclusions

In this work, we have computed the electronic properties for the interfaces of semipolar plane AlN(1 $\bar{1}$01)/C heterostructures by the first-principles calculations. Both clean and hydrogenated diamond (100) surface are also examined. The DOSs dramatically increase at the Fermi level inducing insulator-metal transition for the stable semi-polar plane AlN(1 $\bar{1}$01)/C heterostructures. Such a transition results from the hybrid of N 2p and C 2s2p orbital electrons. The quantity of charge transferred at the interface is suppressed by the introduction of H. The maximum valence-band offset reaches 2.0 eV, and corresponding conduction-band offset is 1.3 eV for the semi-polar plane N–AlN(1 $\bar{1}$01)/HC(100) heterostructure. And the minimum valence-band offset is 0.7 eV, and corresponding conduction-band offset is 0 eV for the semi-polar N–AlN/C(100) heterostructure. The unique band alignment of this Type-II staggered system with the higher CBO and VBO values of the semi-polar AlN/HC(100) heterostructure provides an avenue to the development of robust high-power high-frequency power devices.

References

[1] Nebel C E 2003 *Nat. Mater.* **2** 431
[2] Nebel C E, Sauerer C, Ertl F, Stutzmann M, Graeff C F O, Bergonzo P, Williams O A and Jackman R 2001 *Appl. Phys. Lett.* **79** 4541
[3] Volpe P N, Muret P, Pernot J, Omnès F, Teraji T, Koide Y, Jomard F, Planson D, Brosselard P, Dheilly N, Vergne B and Scharnholz S 2010 *Appl. Phys. Lett.* **97** 223501
[4] Daicho A, Saito T, Kurihara S, Hiraiwa A and Kawarada H 2014 *J. Appl. Phys.* **115** 223711
[5] Taniyasu Y, Kasu M and Makimoto T 2006 *Nature* **441** 325
[6] Kawarada H, Tsuboi H, Naruo T, Yamada T, Xu D, Daicho A, Saito T and Hiraiwa A 2014 *Appl. Phys. Lett.* **105** 013510
[7] Hirama K, Taniyasu Y and Kasu M 2011 *Appl. Phys. Lett.* **98** 011908
[8] Imura M, Hayakawa R, Watanabe E, Liao M Y, Koide Y and Amano H 2011 *Phys. Status Solidi RRL* **5** 125
[9] Silvestri L, Cervenka J, Prawer S and Ladouceur F 2013 *Diamond Relat. Mater.* **31** 25
[10] Silvestri L and Ladouceur F 2016 *J. Phys. Chem. Lett.* **7** 1534
[11] van der Weide J, Zhang Z, Baumann P K, Wensell M G, Bernholc J and Nemanich R J 1994 *Phys. Rev. B* **50** 5803
[12] Furthmüller J, Hafner J and Kresse G 1996 *Phys. Rev. B* **53** 7334
[13] Sque S J, Jones R and Briddon P R 2006 *Phys. Rev. B* **73** 085313
[14] Hassan Mir M and Larsson K 2014 *J. Phys. Chem. C* **118** 22995
[15] Takeuchi D, Koizumi S, Makino T, Kato H, Ogura M, Ohashi H, Okushi H and Yamasaki S 2013 *Phys. Status Solidi A* **210** 1961
[16] Hung A, Russo S P and Mcculloch D G 2004 *J. Chem. Phys.* **120** 4890
[17] Qiao Z J, Chen G D, Ye H G, Wu Y L, Niu H B and Zhu Y Z 2012 *Chin. Phys. B* **21** 087101
[18] O'Donnell K M, Martin T L, Fox N A and Cherns D 2010 *Phys. Rev. B* **82** 115303
[19] Long R, Dai Y, Yu L, Jin H and Huang B 2008 *Appl. Surf. Sci.* **254** 6478
[20] Wu K P, Ye J D, Tang K, Qi J, Zhu S M and Gu S L 2015 *Comput. Mater. Sci.* **109** 225
[21] Deng H X, Luo J W and Wei S H 2015 *Phys. Rev. B* **91** 075315
[22] Sinai O, Hofmann O T, Rinke P, Scheffler M, Heime G and Kronik L 2015 *Phys. Rev. B* **91** 075311
[23] Monkhorst H J and Pack J D 1976 *Phys. Rev. B* **13** 5188
[24] Gan L Y, Zhao Y J, Huang D and Schwingenschlögl U 2013 *Phys. Rev. B* **87** 245307
[25] Cheng Y W, Tang F L, Xue H T, Liu H X, Gao B and Feng Y D 2016 *Mater. Sci. Semicond. Process.* **45** 9
[26] O'Donnell K M, Edmonds M T, Tadich A, Thomsen L, Stacey A, Schenk A, Pakes C I and Ley L 2015 *Phys. Rev. B* **92** 035303
[27] Kolpak A M and Beigi S I 2012 *Phys. Rev. B* **85** 195318
[28] Luo X H, Bersuker G and Demkov A A 2011 *Phys. Rev. B* **84** 195309
[29] Deng H X, Li S S and Li J B 2010 *J. Phys. Chem. C* **114** 4841
[30] Berland K and Hyldgaard P 2014 *Phys. Rev. B* **89** 035412
[31] Amico N R D, Cantele G, Perroni C A and Ninno D 2015 *J. Phys.: Condens. Matter* **27** 015006
[32] Flage-Larsen E, Løvvik O M, Fang C M and Kresse G 2013 *Phys. Rev. B* **88** 165310
[33] Gudmundsdóttir S, Tang W J, Henkelman G, Jónsson H and Skúlason E 2012 *J. Chem. Phys.* **137** 164705
[34] Wu K P, Ma W F, Sun C X, Wang Z G, Ling L Y and Chen C Z 2018 *Comput. Mater. Sci.* **145** 191
[35] Al-Allak H M and Clark S J 2001 *Phys. Rev. B* **63** 033311
[36] Peng Q, Wang Z Y, Sa B S, Wu B and Sun Z M 2016 *ACS Appl. Mater. Interfaces* **8** 13449
[37] Van de Valle C G and Martin R M 1987 *Phys. Rev. B* **35** 8154
[38] Lin L and Robertson J 2009 *Appl. Phys. Lett.* **95** 012906
[39] Hirose K, Sakano K, Nohira H and Hattori T 2001 *Phys. Rev. B* **64** 155325
[40] Sharia O, Demkov A A, Bersuker G and Lee B H 2007 *Phys. Rev. B* **75** 035306
[41] Liu J W, Liao M Y, Imura M and Koide Y 2012 *Appl. Phys. Lett.* **101** 252108
[42] Mendoza F, Makarov V, Weiner B R and Morell G 2015 *Appl. Phys. Lett.* **107** 201605
[43] Baca A G, Armstrong A M, Allerman A A, Douglas E A, Sanchez C A, King M P, Coltrin M E, Fortune T R and Kaplar R J 2016 *Appl. Phys. Lett.* **109** 033509
[44] Liu S H, Yang S, Tang Z K, Jiang Q M, Liu C, Wang M J, Shen B and Chen K J 2015 *Appl. Phys. Lett.* **106** 051605
[45] Grabowski S P, Schneider M, Nienhaus H, Mönch W, Dimitrov R, Ambacher O and Stutzmann M 2001 *Appl. Phys. Lett.* **78** 2503
[46] Wu C I and Kahn A 1999 *Appl. Phys. Lett.* **74** 546
[47] Nemanich R J, Benjamin M C, Bozeman S P, Bremser M D, King S W, Ward B L, Davis R F, Chen B, Zhang Z and Bernholc J 1995 *Mater. Res. Soc. Symp. Proc.* **395** 777
[48] Crawford K G, Cao L, Qi D C, Tallaire A, Limiti E, Verona C, Wee A T S and Moran D A J 2016 *Appl. Phys. Lett.* **108** 042103